Advances in Grating-Coupled Hybrid Surface Plasmon Resonance at Flat Metal–Analyte Interface

F. Haddad[a], A. Cherifi[b,*], M. Nedjari[c], B. Bouhafs[d] and A. Bezza[d]

[a] *Department of Material Science, Science and Technology Faculty, University of Amenokal Hadj Moussa Ag Akhamouk, Tamanrasset 11000, Algeria*
[b] *Department of Physics, Faculty of Exact Sciences and Informatics, Hassiba Benbouali University of Chlef, Chlef 02000, Algeria*
[c] *Laboratory of Materials and Reactive Systems, Djillali Liabes University, Sidi Bel Abbes 22000, Algeria*
[d] *Theoretical Physics Laboratory, Faculty of Sciences, University of Tlemcen, Tlemcen 13000, Algeria*

Received: 19.10.2024 & Accepted: 18.12.202

Doi: 10.12693/APhysPolA.147.90 *e-mail: cherifi_physics@yahoo.com

In this paper, we theoretically investigate the sensing characteristics of a metallic grating-coupled surface plasmon resonance sensor with the objective of showing their influence on the grating parameters. For comparison, the optical responses of silver (Ag), gold (Au), and copper (Cu), as plasmonic material layers, are separately adopted in the Kretschamann approach. The reflectivity of each plasmonic layer coated on top of a glass prism is analyzed using the wavelength interrogation method. The optical responses of the considered configurations are analyzed, where the impact parameters are related to the grating parameters (height, width, and periodicity) and layer thickness that have been suitably optimized. Additionally, the excitation angle of incident light is fixed in the range from 26° to 66°, and the outer medium refractive index is assumed in the range from 1.33 to 1.34. Thus, the obtained results reveal that the proposed structures allow for a remarkable coupling between surface plasmon resonance and localized surface plasmon resonance, whose functionality as efficient refractive index sensors is characterized by improved wavelength sensitivity in the range $\lambda \simeq 400$–100 nm, high figure of merit, and the narrowest spectral full width at half maximum of the resonant plasmonic response. Such preferential limits of the performance parameters should make the suggested multilayer approaches based on Ag, Au, and Cu a suitable choice for detection applications.

topics: surface plasmon resonance (SPR), metallic grating, wavelength interrogation method, refractive index (RI) sensor

1. Introduction

Surface plasmon resonance (SPR) phenomenon is important in the development of many optical devices, including chemical and biochemical sensors such as surface-enhanced Raman spectroscopy (SERS) [1], data storage and solar cells, waveguides, and surface enhancers that depend on nonlinear mixers [2, 3], etc. From a historical standpoint, such resonant optical interface phenomenons were initially observed in 1902 by Wood as anomalies on the light spectrum reflected from a metallic grating. The specificity of such Wood's anomalies is the apparition of dark bands [4]. Later, the anomalies were proved to be correlated with electromagnetic surface waves [5]. After that, a series of research appeared explaining the loss of energy in metallic surfaces [6–9], and then the anomalies ended up being called surface plasmon polariton by Cunningham et al. [10]. Therefore, we find a major trend towards using nano-thin films that are cost-effective and have excellent optical properties, in order to improve performances of SP biosensors [11]. Many researchers have proposed more advanced plasmon coupling techniques, such as the nanoparticles and molecules mixes [12], diffraction multiplexing [13], and coupling in a helical layer [14]. However, these methods, which are based on angles, contain technical parameters that we cannot control, and for this reason, researchers resorted to a method of connecting surface plasmons (SPs) using a periodic network with only a wavelength for a specified angle, which leads to the integration of light into surface plasmon polaritons (SPPs). We mention here recent works, including a comparison of rectangular and sinusoidal periodic lattices [15] and fabricating the aluminum (Al) metasurface interspersed

with an elastomer nanosheet with a film thickness of 400 nm [16, 17]. H. Fasseaux et al. [18] ran the Jones formula on gold-coated tilted fiber Bragg gratings (TFBG) to recover the polarization that gives optimal plasmonic excitation for phase and amplitude measurements. Transverse magneto-photon transport effect (TMPTE) can be investigated in comb-like lattices [19], and surface geometry in the form of a superposition of harmonic Fourier components [20]. Also, researchers are still pursuing the path of using the prism to provide coupling between nanostructure and SPP for SPR sensors. It is the most commonly used way due to its high sensitivity and ease of use [21–29]. Using these devices, we find the plasmonic refractive index (RI). Therefore, there is a competition between researchers to design an RI–plasmonic sensor with the highest sensitivity and figure of merit (FOM) and an easy manufacturing process in various applications, which would lead to meeting the future needs of the refractive index (RI) sensor.

In this study, we report the analysis of the optical response of a plasmonic structure, which makes it possible to study the effects in wavelength interrogation of the spread of the media, and we use the refractive index sensing medium based on noble metal grating in the Kretschmann approach to evaluate performance parameters of the structure-based surface plasmon generation and clarify additional associated phenomena of SPs. We study the dispersive properties of Ag, Au, and Cu gratings as active materials coated on prism coupling to significantly reduce the full width at half maximum (FWHM), thus improving the FOM, and compare their respective results.

2. Design parameters of SPR sensor and method

Material properties in the frequency domain should be considered because they essentially govern fundamental processes such as dispersion, scattering, and absorption during the propagation of an external electromagnetic wave. Thus, as illustrated in Fig. 1, the optical-system-based SPR sensor comprises three layers, namely glass prism, metallic grating, metallic film, and sensing medium. Here, the first incident medium is the glass prism of RI, $n_p = 1.5$. For the metallic film, i.e., Ag/Au/Cu, the complex dielectric permittivity is described by the Drude model. The formula is given as [30–33]

$$\varepsilon_M(\omega) = 1 - \frac{\omega_p^2}{\omega^2 - \gamma^2} + i\frac{\gamma\omega_p^2}{\omega^2 - \gamma^2} \tag{1}$$

with ω_p, γ, and ω representing the plasma frequency, collisional frequency, and angular frequency of operating light, respectively. The parameters of the metallic grating are noted as length (d_f), periodicity (A), and width (w). When certain

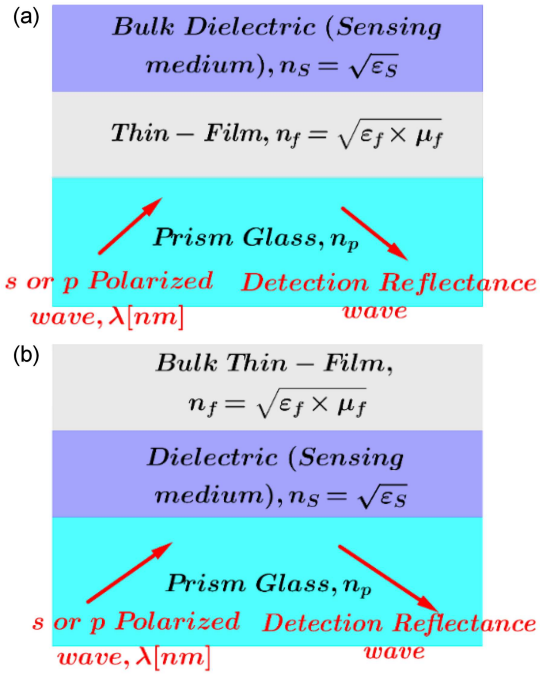

Fig. 1. (a) The Kretschmann configuration and (b) the Otto configuration.

conditions are met, excitation of the species occurs. There are two methods to examine surface plasmon excitation, namely wavelength interrogation of incident light and incident angle interrogation. Each method is characterized by certain restrictions and changes depending on the optical and geometric parameters of the metal surface. Prism coupling is one of the most common techniques (see Fig. 1a and b), where total internal reflection is used to transfer the propagation of a wave at a metal/ephemeral SP interface to the brown surface, which leads to an increase in its parallel vector to the refractive index of the prism, so the SPs at the metal/dielectric interface are excited by an evanescent optical field that is created. When total internal reflection of an incoming light wave occurs, we observe two types of multilayer configurations for surface plasmon observations, which are the configurations proposed by Kretschmann–Raether [6] and Otto [7]. In the first configuration, a metal layer is in contact with an optical coupler, such as a prism, semi-cylinder or two prisms. In the second configuration, the metallic layer is separated from the coupler by a dielectric gap of an order of wavelength thickness [25]. In this case, the surface plasmons at the metal/dielectric interface can be excited by an evanescent optical field, which is obtained when the total reflection of an incident light wave occurs. The optical responses of the above valuable configurations are based on Fresnel theory and the boundary conditions of electric fields for incident wave propagation on the interfaces in different environments media.

3. Results and discussions

In the Kretshmann configuration, SPs are excited in a fully diluted ATR reflector. A rectangular metal nanosheet is located directly above the prism in our approaches. Otherwise, no intermediate metal layer is included between the nanostructured metal film and the prism. We assume that the nanostructured Ag/Au/Cu grating films are irradiated at a fixed incident angle and illuminated by a light beam with transverse magnetic polarization. The wavelength of the light beam is considered in the range from 400 to 1100 nm. The geometry is oriented in the x, z-plane and has an infinite dimension according to the x direction. Symbols of the three-layer system is seen in Fig. 2 (layer 1 — prism, layer 2 — Ag/Au/Cu grating films). Light falls on the nanostructured metal layer through a prism with a high refractive index. The thickness of the nanostructured metal film is d_f. We use the properties of the effective medium for one-dimensional (1D) gratings, which describe well the grating metallic structures through general materials and geometric parameters. They are defined as

$$\varepsilon_f(\lambda) = \frac{A}{A\varepsilon_M^{-1} + w\left(n_S^{-2} - \varepsilon_M^{-1}(\lambda)\right)},$$
$$\mu_f(\lambda) = 1, \tag{2}$$

where the periodicity A is the parameter of the nanostructured metal film, and w is the slit width [34]. An insulating material is used to fill the cracks; in the case of this configuration, the SPR response occurs at an incidence wavelength, λ_{SP}, which can be predicted from the reflection behavior. We try to reach a clear understanding of the influence of physical phenomena in the case of rectangular metal nanograting, and their implementation is analyzed through three main parameters: reflection intensity, half-height width, and detection accuracy, where the electromagnetic wavelength is located by the index prism. To generate a resonant excitation observable on the reflectivity, the incident wave of transverse magnetic (TM) polarization undergoes total internal reflection at the prism-metal interface.

3.1. SP change with incidence angle θ_i and the wavelength λ

The electromagnetic wave is incident on a lattice of the dielectric layer of the geometric interface in this geometric mode, where the incident (prism) medium of the structure is quasi-infinite (the term "quasi-infinite emergent medium" refers to a dielectric medium with a variety of optical properties). Analytically using the theoretical technique for light reflection at the prism–Ag/Au/Cu lattice interface of the structure by adopting different incidence

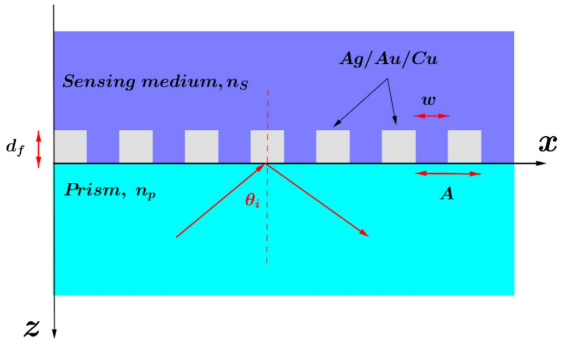

Fig. 2. The Kretschmann configuration — a nanostructured 1D grating layer between the prism of a high index and the sensing medium with an index of refraction of 1.3325.

angles, θ_i [°] (see Fig. 3), we show how wave reflectivity and structure change interact with the change in incidence angle. Otherwise, refraction over a wide spectral range of 400–1100 nm was used to produce successful coupling with the difference of two consecutive values equal to 0.023 nm. We can see that all reflectance spectra present spectral resonance under the conditions and shift from right to left, which even mimics the effect of a change in the minimum reflectance. The resonance condition (λ_{SPR}) versus the incidence angle θ_i for Ag, Au, and Cu, respectively, is given by the following polynomial equations:

- for Ag,

$$\lambda_{\mathrm{SPR}}(\theta_i)\,[\mathrm{nm}] = (-0.10986\,\theta_i^2 - 2.2466\,\theta_i + 1021.4) \pm 0.91029, \tag{3}$$

- for Au,

$$\lambda_{\mathrm{SPR}}(\theta_i)\,[\mathrm{nm}] = (-0.11031\,\theta_i^2 - 2.1523\,\theta_i + 1014.1) \pm 1.1738, \tag{4}$$

- for Cu,

$$\lambda_{\mathrm{SPR}}(\theta_i)\,[\mathrm{nm}] = (-0.1174\,\theta_i^2 - 1.5714\,\theta_i + 1006.8) \pm 2.585. \tag{5}$$

We also notice a change with a decrease in the minimum reflection from left to right for the Ag and Au grating, i.e., from the resonance of visible to infrared wavelengths, in contrast to the copper grating. In this work, we are interested in copper grating, which is less expensive than other plasmonic metals, and we compare it with them, as we said previously. The minimum reflectance is the smallest at infrared wavelengths for a copper grating, and for this reason, we fix the incident angle to correspond to one of these wavelengths, for example, $\theta_i = 28°$, and we obtain SPR wavelengths of 872.1 nm, 867.7 nm, and 872 nm. The minimum reflectance, MR, is 6.794%, 8.947%, and 2.747%, corresponding to Ag grating, Au grating, and Cu grating, respectively.

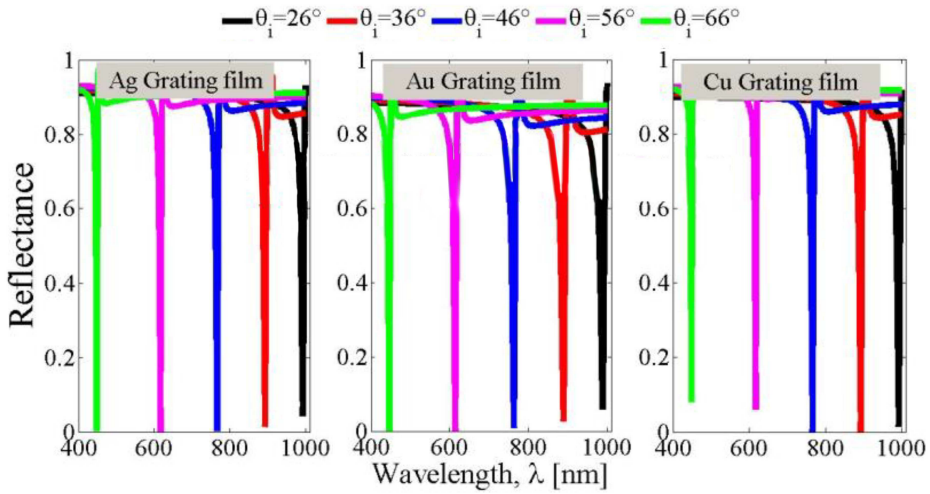

Fig. 3. Reflectance curve of Ag/Au/Cu grating as a function of incidence angle, θ_i, with the Ag/Au/Cu grating film thickness of $d_f = 41$ nm, periodicity of $A = 500$ nm, and slit width of $w = 2$ nm. The refractive indices used are: $n_P = 1.5$, $n_f = \sqrt{\varepsilon_f \mu_f}$ and $n_S = 1.3325$; $\varepsilon_f = \mu_f = 1$.

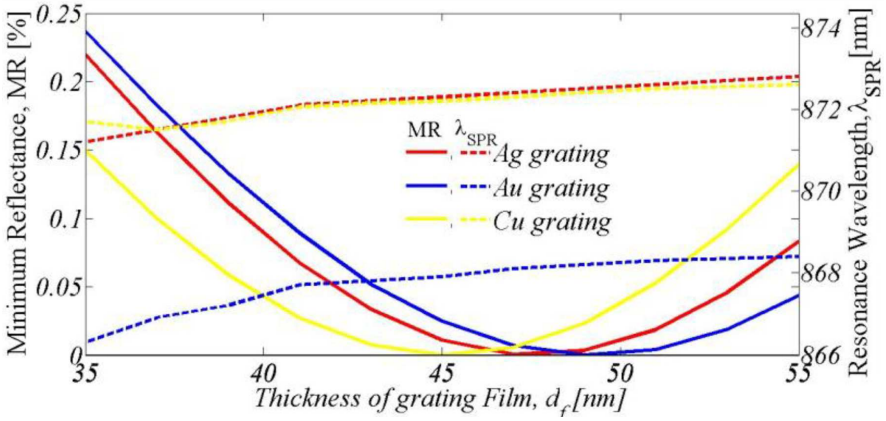

Fig. 4. Minimum reflectance MR and resonance wavelength λ_{SPR} as a function of the thickness of film d_f for Ag/Au/Cu with: $d_f \in [35, 55]$ nm, $A = 500$ nm, $w = 2$ nm, n_d =1.3325, and $\theta_i = 28°$.

3.2. Changes in SP effect on the thickness of the grating film

Figure 4 shows the calculated different values of the minimum reflectance intensity and the SPR wavelength at the wavelengths previously distinguished for each structure while changing the thickness of the grating layer from 35 to 55 nm, while maintaining the values of the other variables same as in Fig. 3 and $\theta_i = 28°$. Note that the reflection intensities with continuous curves are identical in terms of variation, each decreasing as a function of the thickness of the grating layer up to values of $d_{\mathrm{Ag}} = 47$ nm, $d_{\mathrm{Au}} = 49$ nm, and $d_{\mathrm{Cu}} = 45$ nm, which correspond to Ag grating, Au grating, and Cu grating, as small as 0.005%, 0.001%, and 0.003%, respectively. Then the trend changes with an increase at the resonance wavelengths of 872.1 nm, 867.7 nm, and 872 nm, respectively.

3.3. Influence of periodicity and slit width

Next, we examine the effect of each periodicity A. The slit width w depends on the intensity and the wavelength of the SPR mode resonance maintained by the structure while maintaining the previous characteristic magnitudes for each structure. So when we change value w (see Fig. 5a), we find that the peak reflectance decreases to the values of $MR_{\mathrm{Ag}} = 5.369{\times}10^{-4}\%$, $MR_{\mathrm{Au}} = 1.345{\times}10^{-4}\%$, and $MR_{\mathrm{Cu}} = 3.742 \times 10^{-4}\%$ at $w_{\mathrm{Ag}} = 2.4$ nm, $w_{\mathrm{Au}} = 2.2$ nm, and $w_{\mathrm{Cu}} = 2$ nm, which corresponds to the resonance wavelengths of 872.8 nm, 868.4 nm, and 872.2 nm for Ag grating, Au grating, and Cu grating, respectively. For structures based on the three types of metal-gratings previously described, the minimum of their reflected intensities reaches a value close zero. Then, after choosing the appropriate thicknesses for slit width, w, and

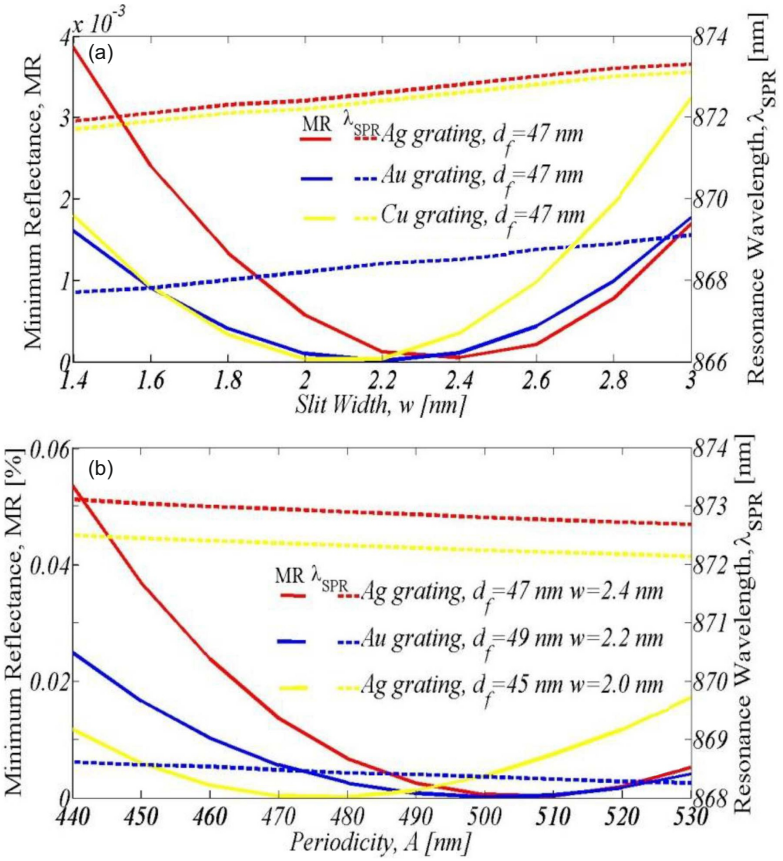

Fig. 5. Minimum reflectance, MR, and resonance wavelength, λ_{SPR}, as a function of slit width, w, and periodicity, A, for Ag/Au/Cu with: (a) $w \in [1.4, 3]$ nm, $d_{\mathrm{Ag}} = 47$ nm, $d_{\mathrm{Au}} = 49$ nm, and $d_{\mathrm{Cu}} = 45$ nm, (b) $A \in [440, 520]$ nm, $w_{\mathrm{Ag}} = 2.4$ nm, $w_{\mathrm{Au}} = 2.2$ nm, and $w_{\mathrm{Cu}} = 2$ nm; the other parameters are the same as in Fig. 4.

other characteristic quantities mentioned previously, the extent of the effect of periodicity, A, is considered (see Fig. 5b). The reflectance peak decreases to the value of $MR_{\mathrm{Ag}} = 2.679 \times 10^{-4}\%$, $MR_{\mathrm{Au}} = 1.086 \times 10^{-4}\%$, and $MR_{\mathrm{Cu}} = 1.287 \times 10^{-4}\%$, which corresponds to the SPR wavelengths of 872.1 nm, 867.7 nm, and 872 nm at $A_{\mathrm{Ag}} = 510$ nm, $A_{\mathrm{Au}} = 500$ nm, and $A_{\mathrm{Cu}} = 480$ nm, which also corresponds to the resonance wavelengths of 872.76 nm, 868.36 nm, and 872.32 nm for Ag grating, Au grating, and Cu grating, respectively. For both quantities, we find that they have a clear impact on the structural results, in contrast to what some researchers have found in the visual field.

3.4. SP variation with the refractive index of sensing medium

Figure 6 shows simulated spectra transmitted for different RI and detection media. It can be seen that varying the RI in the wide range from 1.32 to 1.35 causes: (i) a linear change in the resonance wavelength, (ii) a slight change in the FWHM of the resonance mode with two ranges of 8–10 nm and 8–9 nm in the cases of Au grating and Cu grating, respectively. In contrast to Ag grating, we find a noticeable change in the 6th-degree polynomial with ranges of 6.14–6.15 nm, and (iii) the intensity of the reflection decreases and increases with the limit depth of each structure.

It should be noted here that the intrinsic properties associated with different types of resonance modes are closely related to the nature of the medium and the geometric quantities constituting the structure in question.

Based on the previous data, analytical dependencies between the intrinsic characteristics retrieved from p-reflectivity curves versus influence parameters can be derived as follows:

(i) Dip depth of p-reflectivity (MR [%]) versus the RI (n_S) of sensing environment reflects

$$MR_{\mathrm{Ag}}(\times 10^{-4}) = 14.02 \sin(102.25\, n_S + 0.92) + 14.823; \quad (6)$$

(ii) Resonance condition (λ_{SPR} [nm]) versus the RI of sensing environment reflects

$$\lambda_{\mathrm{SPR}}\,(\mathrm{Ag}) = (-653.76\, n_S + 1744.6) \pm 1.2363, \quad (7)$$

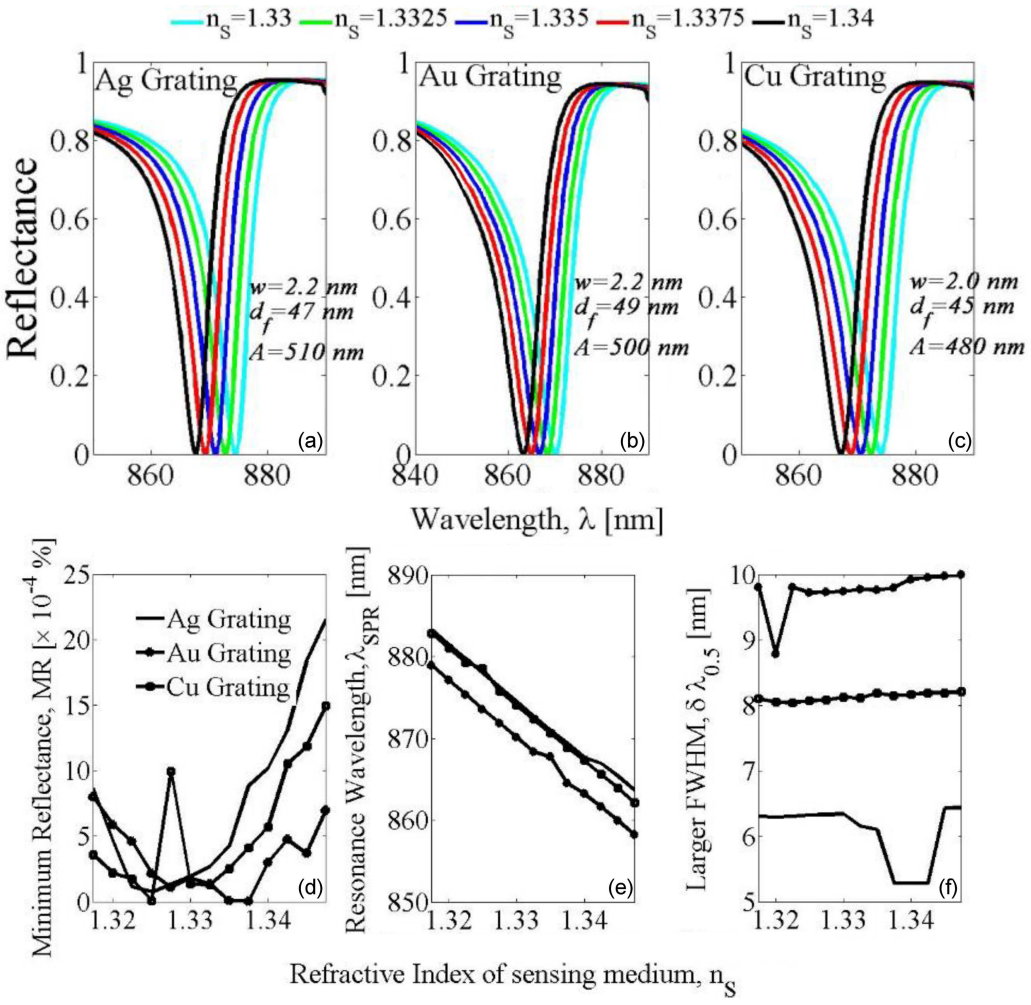

Fig. 6. (a–c) Reflectance spectra with changing RI (1.33–1.34) with grating film at periodicity $A_{\mathrm{Ag}} = 510$ nm, $A_{\mathrm{Au}} = 500$ nm, and $A_{\mathrm{Cu}} = 480$ nm; the other parameters are the same as in Fig. 4b. (d–f) Variation of minimum reflectance (MR), resonance wavelength, and larger FWHM, respectively, as a function of RI (1.32–1.35) of the sensing medium; the other parameters are the same as in Fig. 5.

TABLE I

Variation figure of merit as a function of the RI (1.32–1.34) of sensing medium; the other parameters are the same as in Fig 6a; RIU is the refractive index unit.

	n_S [RIU]								
	1.32	1.3225	1.325	1.3275	1.33	1.3325	1.335	1.3375	1.34
$\mathrm{FoM_{Ag}}$ [$\mathrm{RIU^{-1}}$]	103.91	103.75	103.42	103.14	103.14	106.31	107.17	123.86	123.79
$\mathrm{FoM_{Au}}$ [$\mathrm{RIU^{-1}}$]	78.37	70.22	70.82	70.80	70.71	70.47	70.51	78.26	69.36
$\mathrm{FoM_{Cu}}$ [$\mathrm{RIU^{-1}}$]	86.19	86.19	85.94	85.78	85.93	85.52	84.74	85.19	84.96

$$\lambda_{\mathrm{SPR}}\,(\mathrm{Au}) = (-688.47\,n_S + 1785.9) \pm 1.1473, \quad (8)$$

$$\lambda_{\mathrm{SPR}}\,(\mathrm{Cu}) = (-693.52\,n_S + 1796.6) \pm 0.9383; \quad (9)$$

(iii) The full width at half maximum (FWHM) of a reflectance dip ($\Delta\lambda_{0.5}$ [nm]) versus the RI of the sensing environment reflects

$$\Delta\lambda_{0.5}\,(\mathrm{Ag}) = \sum_{i=1}^{i=7} P_i\, n_S^{i-1} \pm 0.48081. \quad (10)$$

Here, $P_1 = -3.32 \times 10^{12}$, $P_2 = 1.496 \times 10^{13}$, $P_3 = -2.81 \times 10^{13}$, $P_4 = 2.812 \times 10^{13}$, $P_5 = -1.584 \times 10^{13}$, $P_6 = 4.756 \times 10^{12}$, and $P_7 = -5.952 \times 10^{11}$.

As such, a small fluctuation in the RI of the sensing environment reflects how precisely the sensor detects the resonance condition and its shift. This value allows the determination of resulting sensitivity, $S_\lambda = \delta\lambda_{\mathrm{SP}}/\delta n_S$ [35], and the figure of merit is FoM $= S_\lambda/\mathrm{FWHM}$ [36]. As displayed in Fig.6a–c, for the three SPR sensors

analyzed, the increasing variation from 1.33 to 1.34 of the analyte refractive index, produces a substantial decreasing shift in the spectral position, λ_{SPR} of the SPR mode. According to the analytical expressions in 7–9, Cu grating presents the highest spectral sensitivity compared to that achieved with Ag grating and Au grating. If we take into account the selectivity, regarding the limit value of FoM shown in Table I, Ag grating as an SPR sensor refractive index is preferable than Cu grating and Au grating.

4. Conclusions

Through the theoretical study, we found that plasmonic lattice devices can open a new path for developing sensing applications based on the ability to exhibit a remarkable coupling between SPR and localized surface plasmon resonance (LSPR) generation. A comparative study with Ag, Au, and Cu grating sensing at infrared wavelengths is presented. We determined the geometric quantities according to the fundamental plasmonic mode and in line with practical devices. The possibility of using multilayers as a refractive index sensor for aqueous solutions has been largely demonstrated. The sensitivity of all three metals was calculated, and Cu was found to be the most efficient. It should be noted that a compromise of a few nm/RIU is needed for a more stable and less expensive 1D grating device, early sensing, and efficient sensing using Cu grating. Moreover, it is less expensive for others. However, one can use an Ag grating as well with little compromise on the sensitivity and the best figure of merit for the designed sensor.

References

[1] W.L. Barnes, A. Dereux, T.W. Ebbesen, *Nature* **424**, 824 (2003).

[2] S. Palomba, L. Novotny, *Phys. Rev. Lett.* **101**, 056802 (2008).

[3] S.A. Maier, *Plasmonics: Fundamentals and Applications*, Vol. 1, Springer, New York 2007.

[4] R.W. Wood, *Lond. Edinb. Dubl. Phil. Mag. J. Sci.* **4**, 396 (1902).

[5] U. Fano, *J. Opt. Soc. Am.* **31**, 213 (1941).

[6] E. Kretschmann, H. Raether, *Z. Naturforsch. A* **23**, 2135 (1968).

[7] A. Otto, *Z. Phys. A Hadrons Nucl.* **216**, 398 (1968).

[8] R.H. Ritchie, E.T. Arakawa, J.J. Cowan, R.N. Hamm, *Phys. Rev. Lett.* **21**, 1530 (1968).

[9] D. Pines, *Rev. Mod. Phys.* **28**, 184 (1956).

[10] S.L. Cunningham, A.A. Maradudin, R.F. Wallis, *Phys. Rev. B* **10**, 3342 (1974).

[11] A. Bouhenna, O. Zeggai, J. Wekalao, A. Achour, H. Mouloudj, *Plasmonics* **2024**, 1 (2024).

[12] R. Zaier, M. Bancerek, K. Kluczyk-Korch, T.J. Antosiewicz, *Nanoscale* **16**, 12163 (2024).

[13] J. Zhang, L. Zhang, W. Xu, *J. Phys. D Appl. Phys.* **45**, 113001 (2012).

[14] S.F.J.L.Z. Hsieh, L.B. Chang, C.C. Hsieh, C.M. Wu, *J. Med. Biol. Eng* **26**, 149 (2006).

[15] T. Iqbal, S. Noureen, S. Afsheen, M.Y. Khan, M. Ijaz, *Opt. Mater.* **99**, 109530 (2020).

[16] H. Kumagai, T. Fujie, K. Sawada, K. Takahashi, *Adv. Opt. Mater.* **8**, 1902074 (2020).

[17] Y. Guo, N.M. Singh, C.M. Das, K. Wei, K. Li, P. Coquet, K.-T. Yong, *Optik* **224**, 165690 (2020).

[18] H. Fasseaux, M. Loyez, K. Chah, C. Caucheteur, *Opt. Express* **30**, 34287 (2022).

[19] O.V. Borovkova, M.A. Kozhaev, H. Hashim, A.A. Kolosova, A.N. Kalish, S.A. Dagesyan, A.N. Shaposhnikov, V.N. Berzhansky, V.I. Belotelov, *Opt. Mater. Express* **12**, 573 (2022).

[20] A.V. Dyshlyuk, A. Proskurin, A.A. Bogdanov, O.B. Vitrik, *Nanomaterials* **13**, 2091 (2023).

[21] K. Matsubara, S. Kawata, S. Minami, *Appl. Opt.* **27**, 1160 (1988).

[22] S. Lofas, M.Malmqvist, I. Ronnberg, E. Stenberg, B. Liedberg, I. Lundström, *Sens. Actuators B* **5**, 79 (1991).

[23] J. Homola, *Sens. Actuators B Chem* **41**, 207 (1997).

[24] F.C. Chien, S.J. Chen, *Biosens. Bioelectron.* **20**, 633 (2004).

[25] A. Bezza, A. Cherifi, B. Bouhafs, *Revista Mexicana de Física* **69**, 021002-1 (2023).

[26] A. Cherifi, B. Bouhafs, *Int. J. Sensors Wireless Commun. Control* **10**, 1001 (2020).

[27] A. Cherifi, B. Bouhafs, *Mater. Res. Express* **4**, 125009 (2017).

[28] M. Bendjebbour, A. Cherifi, B. Bouhafs, *Photon. Sens.* **10**, 113 (2020).

[29] A. Cherifi, B. Bouhafs, *Photon. Sens.* **7**, 199 (2017).

[30] R. Umeda, C. Totsuji, k. Tsuruta et al., *Mater. Trans.* **50**, 994 (2009).

[31] B. Ung, Y. Sheng, *Opt. Express* **15**, 1182 (2007).

[32] A.D. Rakić, A.B. Djurišić, J.M. Elazar, M.L. Majewski, *Appl. Opt.* **37**, 5271 (1998).

[33] J.E. Laurens, K.E. Oughstun, in: *Ultra-Wideband Short-Pulse Electromagnetics*, IEEE, 1999, p. 243.

[34] S. Tang, B. Zhu, M. Jia, Q. He, S. Sun, Y. Mei, L. Zhou, *Phys. Rev. B* **91**, 174201 (2015).

[35] F. Wang, Y. Wei, Y. Han, *Sensors* **23**, 6617 (2023).

[36] P. Berini, *Opt. Express* **14**, 13030 (2006).